Impact of Error Correction on Protection Performance during Geomagnetic Disturbances

Sakis Meliopoulos, Jiahao Xie, George J. Cokkinides
School of Electrical and Computer Engineering, Georgia Institute of Technology
Atlanta, Georgia, USA

***Abstract*—Geomagnetic disturbances (GMD) occur due to solar wind interactions with Earth's magnetic field. The geographically extensive power system is impacted with geometrically induced current (GIC) which are DC like (low frequency 0.0001Hz to 1 Hz). GIC causes half cycle saturation of iron core circuits, subsequent distortion of the current and voltage waveforms and drastically increased losses in transformers. In addition, GIC causes increased reactive power consumption and waveform distortion which may lead to substantial instrumentation channels errors and possible relay mis-operations. Ideally, the secondary voltage and current of instrumentation channels should be an exact replica of the primary quantities. However, the DC voltage generated by GMD would introduce DC flux in iron cores of instrumentation transformers, leading to distorted magnetizing current. The non-sinusoidal magnetizing current will increase significantly as the DC flux increases, leading to gross distortion in measurements. The harmonic components would lead to additional error, because the frequency response of instrumentation channel is frequency dependent. The distorted measurements may compromise the operation of protective relays. Many protective relays are calibrated at base frequency, so the performance of these relays with distorted measurements is worth investigating. In this paper, we analyze the instrumentation channel errors during GMD events and the performance of the relays considering these errors. The reliability of the relays is examined under different error scenarios. We also propose a state estimation based method for instrumentation channel error correction. Unlike the existing approaches for instrumentation channel error correction based on signal processing techniques, the proposed method relies on the detailed modelling of the instrumentation channels. The internal states and primary quantities are estimated via dynamic state estimation. Therefore, the distortions from instrumentation transformers are eliminated. In addition, the proposed method can handle the distortion from power transformers saturation correctly. The simulation results show that the corrected measurements are highly consistent with real primary quantities, and mis-operation of protective relay is avoided.**

***Index Terms*—Dynamic state estimation, current transformer, potential transformer, error correction, protective relay**

I. INTRODUCTION

Geomagnetic disturbances (GMD) occur when increased solar activities influence the earth magnetic field by charged particles released from the Sun. The variation of magnetic field density leads to geomagnetically induced current (GIC), which refers to the induced current flowing through transmission lines and transformer windings. The frequency of GIC is relatively low (0.0001Hz to 1 Hz), which causes half cycle saturation of iron core circuits and subsequent distortion of the current and voltage waveforms. In addition to overheating transformers and other iron core circuits, increase in reactive power consumption, the waveform distortion may lead to substantial instrumentation channels errors and possible relay mis-operations. For example, DC current in the primary of CTs may cause half cycle saturation of CTs and subsequent distorted data into the relays.

The instrumentation channels interface electric power system with high voltage/current and the protective relays with low voltage/current. A typical instrumentation channel includes potential transformers (PT) or current transformers (CT), instrumentation cables, and merging units. Ideally, the secondary voltage and current of instrumentation channels should be exactly proportional to the primary quantities. However, the DC voltage generated by GMD would introduce DC flux in iron cores of instrumentation transformers, leading to distorted magnetizing current. The non-sinusoidal magnetizing current will increase significantly as the DC flux increases, leading to gross distortion in measurements from burden resistor. In addition, other harmonic components would lead to additional error, because the frequency responses of instrumentation channel are different for different harmonics. These distorted measurements risk the operation of protective relays [1]. Many protective relays are calibrated at base frequency, so the performance of these relays with distorted measurements is worth investigation.

Dynamic state estimation based protection (EBP) is an emerging protection technique [2], which integrates all existing measurements in zone protection to improve the reliability of protection scheme and withstand hidden failures. EBP scheme models the entire protection zone using an objective oriented method, which is referred as quadratized dynamic model (QDM). EBP monitors the consistency between measurements and related physically based models. For example, the measurements of voltage, current and temperature from a protection zone should follow Kirchhoff's Current/Voltage Law (KCL/KVL) and thermodynamic laws.

Once internal faults occur in the protection zone, the EBP is able to detect a violation of physical law, and faulted devices can be tripped. Like other relay methods, accurate measurement input is essential to the reliable operation of the EBP. In virtue of the redundant measurements, hidden failures that corrupt the streaming measurements can be detected and eliminated by EBP inherently [2]. However, the distortion introduced by instrumentation channels may hinder the performance of EBP, and error correction methods are needed.

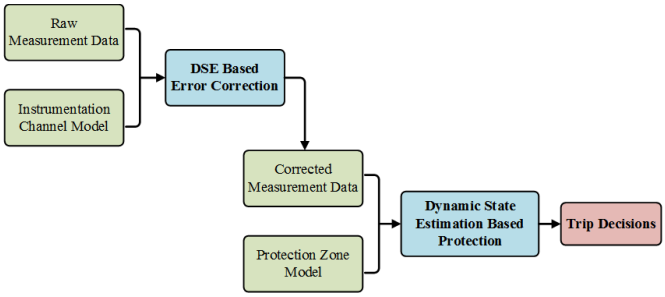

Figure 1. Overview of the proposed error correction procedure for EBP

In this paper, we present a high-fidelity model for simulating the effects of GIC on power systems. The model is based on detailed representation of power system frequency dependent grounding models, low broadband modeling of transmission lines and transformers models with detailed magnetization characteristics [3], [4]. Using this model, we present examples of effects of GMD on the relaying system for different levels of geomagnetically induced currents into the power system via the grounds of the power systems. The examples show that during these events, DC flow in power transformers generates harmonics and the phase currents are distorted with DC and harmonics. The examples also show that relaying instrumentation channels are affected, and these waveforms can generate substantial errors at the relay input. We present a method to correct these errors by using a dynamic state estimation (DSE) [5]. The paper describes the method and presents examples that demonstrate the effectiveness of the method to remove the complex errors introduced by geomagnetically induced currents. Unlike the existing approaches for instrumentation channel error correction based on signal processing techniques[6], [7], the proposed method relies on the detailed modelling of the instrumentation channels. The internal states and primary quantities are estimated via dynamic state estimation. Therefore, the distortions from instrumentation transformers are eliminated. In addition, the proposed method can handle the distortion from power transformers saturation correctly. Instrumentation channel error correction [5] can substantially improve the reliability of protective relays during a GMD event. This error correction scheme enhances the performance of EBP. The overview of the procedure is shown in Figure 1. A DSE process corrects the error introduced in instrumentation channels. The dynamic state estimation accepts the measurements from burden resistors to estimate not only internal states but also the primary side quantities, which are corrected measurements. Next, these corrected values are streamed to EBP.

II. Dynamic State Estimation-Based Protection

The EBP scheme is inspired by differential protection, which monitors the sum of currents flowing into protection zone and ensures the KCL is not violated. In EBP, all existing measurements in protection zone and related physical laws are integrated into a dynamic state estimation process, any violation of physical law indicates the occurrence of an internal fault. In this section, we introduce the standard modeling syntax for the protection zone, the standard measurement model and the state estimation algorithm in EBP.

A. Quadratized Dynamic Model for Protection Zone

In general, the devices in protection zone are described by set of differential equations derived from physical laws. In EBP, we formulate all device model according to a standard syntax in equation (1), which is referred as Quadratized Dynamic Model (QDM). QDM includes the internal variables $x(t)$, and the through variables $i(t)$. Y_{eqx}, D_{eqx} and C_{eqc} are the coefficients for the linear term, differential term and constant term respectively. High order polynomials are quadratized to second order terms by introducing auxiliary variables, and the coefficients are stored in F_{eqxx}.

$$
\begin{aligned}
i(t) &= Y_{eqx1}\mathbf{x}(t) + D_{eqxd1}\frac{d\mathbf{x}(t)}{dt} + C_{eqc1} \\
0 &= Y_{eqx2}\mathbf{x}(t) + D_{eqxd2}\frac{d\mathbf{x}(t)}{dt} + C_{eqc2} \\
0 &= Y_{eqx3}\mathbf{x}(t) + \left\{ \begin{array}{c} \vdots \\ \mathbf{x}(t)^T \left\langle F^i_{eqxx3} \right\rangle \mathbf{x}(t) \\ \vdots \end{array} \right\} + C_{eqc3}
\end{aligned}
\tag{1}
$$

Based on the QDM model of protection zone, measurements models in equation (2) are developed in terms of internal variables $x(t)$. $z(t)$ are measurements from the protection zone. These measurements derived from physical laws are referred as virtual measurements[2]. In addition, we have three other measurements. Actual measurements represent measurements generated from actual meters and sensors; Derived measurements are quantities that are related to other quantities, for which an actual measurement is available; Pseudo measurements are quantities we have assumptions. For example, neutral voltages should be close to zero.

$$
z(t) = Y_x\mathbf{x}(t) + \left\{ \begin{array}{c} \vdots \\ \mathbf{x}(t)^T \left\langle F^i_x \right\rangle \mathbf{x}(t) \\ \vdots \end{array} \right\} + D_x\frac{d\mathbf{x}(t)}{dt} + C \tag{2}
$$

Using numerical integration methods[8], the differential terms are replaced with functions in terms of states at consecutive time steps. As a result, the protection zone models and measurement models are transformed into Algebraic Quadratic Companion Form model (AQCF) in equation (3).

$$z(t,t_m)=Y_{m,x}\mathbf{x}(t,t_m)+\left\{\begin{array}{c}\vdots\\ \mathbf{x}(t,t_m)^T\left\langle F_{m,x}^i\right\rangle\mathbf{x}(t,t_m)\\ \vdots\end{array}\right\}+C_m \quad (3)$$

B. Unconstraint Optimization Method for Dynamic State estimation

$$\min_{x(t)}\ \zeta(t)=\sum_{i=1}^{n}\left(\frac{h_i\left(x(t)\right)-z_i\left(t\right)}{\delta_i}\right)^2 \quad (4)$$

After the construction of the AQCF model, a weighted least square problem is formulated in EBP. Equation (4) is the general form for the unconstraint optimization method for DSE, where n is the total number of measurements, $z_i\left(t\right)$ is the measurement value, $h_i\left(t\right)$ is the measurement i in terms of the states, and δ_i is the standard deviation of the corresponding measurement. To solve problem (4), a Gauss-Newton iterative algorithm is used:

$$x^{v+1}=x^v-(H^TWH)^{-1}H^TW(h(x^v)-z) \quad (5)$$

Where x^v refers to the estimate of the state vector x at iteration v, H is the Jacobian matrix of the measurement equations, and W is the weighting matrix.

$$H=\frac{\partial h(x)}{\partial x}$$

$$W=diag(\cdots,\frac{1}{\delta_i^2},\cdots)$$

By solving the problem in (4),an optimal estimation of the state variables is obtained. The estimated states are substitute into measurement models to get the estimated measurements. Assuming the error in measurements are independent random variables with standard normal, the objective value ζ in equation (4) is distributed according to chi-squared distribution χ^2. Based on this, a metric named as confidence level is available, which indicates the goodness of estimation. The probability of $\chi^2\geq\zeta$,with υ degrees of freedom is named confidence level , which is given by:

$$P=\Pr\left[\chi^2\geq\zeta\right]=1-\Pr\left[\chi^2\leq\zeta\right]=1-\Pr(\zeta,v)$$

A high confidence level suggests the measurement are consistent with physical models, while low confidence level implies the occurrence of internal faults. The trip decision is released based on a user-defined delay time and reset time as shown in (6).

$$trip=\begin{cases}1, \text{ if } \int_{t-t_{reset}}^{t}P(\tau)d\tau>t_{delay}\\ 0, \text{ otherwise}\end{cases} \quad (6)$$

III. Instrumentation Channel Error Correction

In this paper, we propose a state estimation based error correction method for instrumentation channels. The proposed method relies on the physically based instrumentation channel models, the measurements from burden resistors and the dynamic state estimation procedure mentioned in previous section. The approach to model the instrumentation channels is elaborated in this section.

A. Current Instrumentation Channel Measurement Models

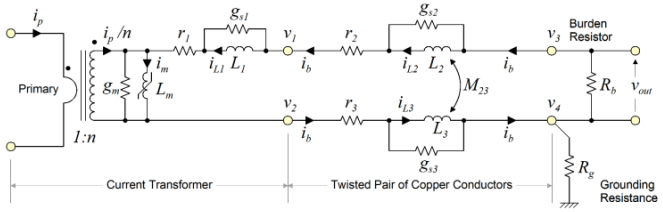

Figure 2. Equivalent circuit of CT's primary current estimation

Figure 2 shows an equivalent circuit for the CT channel error correction, including current transformer with saturable iron core, copper instrumentation cables and burden resistor in merging units. Since the current transformer possess an iron core, the magnetizing inductance L_m is modelled by the nonlinear equation in (7). In which, i_m is the magnetizing current transformed to secondary side, λ is the instantaneous value of flux linkage. Parameters i_0,λ_0,L_0 are the nominal values for magnetizing current, flux linkage and linear inductance respectively. The order n defines the degree of nonlinearity of the model.

$$0=i_m(t)-i_0\left(\frac{\lambda(t)}{\lambda_0}\right)^n-\frac{1}{L_0}\lambda\left(t\right) \quad (7)$$

We choose n=11 for the test case in this paper. Following the standard syntax of QDM model, this equation is quadratized to yield the following quadratized measurement models. Auxiliary variables $y_1\ y_2\ y_3\ y_4$ are introduced to decrease the maximum order of equations to 2.

$$0=y_1(t)-\left(\frac{\lambda(t)}{\lambda_0}\right)^2$$
$$0=y_2(t)-\left(y_1(t)\right)^2$$
$$0=y_3(t)-\left(y_2(t)\right)^2$$
$$0=y_4(t)-y_3(t)\cdot y_1(t)$$
$$0=i_m(t)-i_0\left(\frac{\lambda(t)}{\lambda_0}\right)y_4(t)-\frac{1}{L_0}\lambda\left(t\right)$$

In addition, other physical laws such as KCL and KVL provide more measurement models for CT channels, which is shown in Appendix A. In summary, the current instrumentation channel model consists of 20 measurements, and 15 states. The state variables include:

$$X=[v_1(t)\ v_2(t)\ v_3(t)\ v_4(t)\ e(t)\ \lambda(t)\ y_1(t)\ y_2(t)\ y_3(t)\ y_4(t)$$
$$i_p(t)\ i_m(t)\ i_{L1}(t)\ i_{L2}(t)\ i_{L3}(t)]^T$$

It's worth mentioning that the primary current $i_p\left(t\right)$ is a state variable, so the dynamic state estimation procedure will

reveal the optimal estimation of $i_p(t)$, which is the corrected measurements for current instrumentation channel.

B. Voltage Instrumentation Channel Measurement Models

Following a similar process, we can formulate the measurement models for PT. The parasitic capacitors in primary winding and secondary winding are represented by c_1, c_2 and c_3.

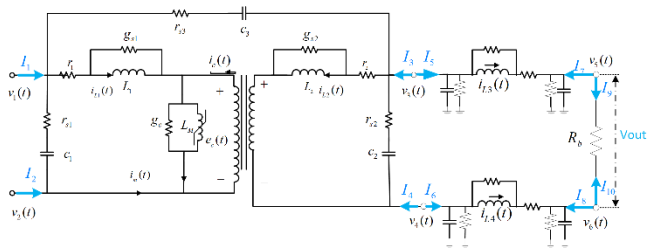

Figure 3. Equivalent circuit of PT's primary voltage estimation

In this test case, there are 20 states, and 21 measurements. The states of model include:

$$X = [v_1(t)\ \ v_2(t)\ \ v_3(t)\ \ v_4(t)\ \ v_5(t)\ \ v_6(t)\ \ i_{L_1}(t)\ \ i_{L_2}(t)$$
$$v_{c1}(t)\ \ v_{c2}(t)\ \ v_{c3}(t)\ \ e_c(t)\ \ i_m(t)\ \ i_c(t)\ \ \lambda(t)$$
$$y_1(t)\ \ y_2(t)\ \ y_3(t)\ \ i_{L3}(t)\ \ i_{L4}(t)\ \ ]^T$$

The voltages at primary side of PT ($v_1(t)$, $v_2(t)$) are state variables, so the dynamic state estimation procedure will reveal the optimal estimation primary voltage, which is the corrected measurements for voltage instrumentation channel. Details of the PT measurement models are shown in Appendix B.

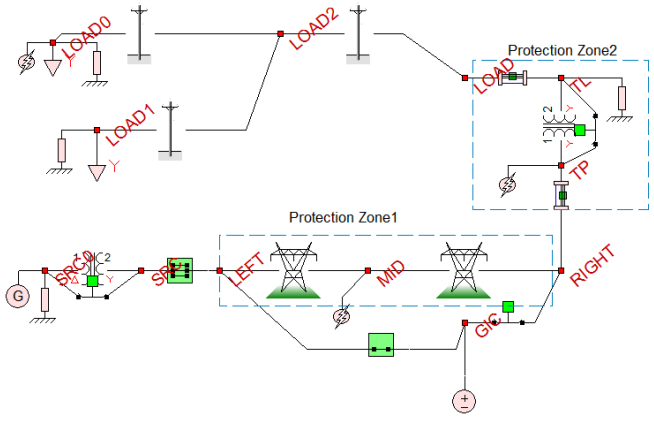

Figure 4. Test system for EBP with error correction

IV. Example Test Results

Example test results are provided here to illustrate the effectiveness of the dynamic state estimation based approach for reliable protection of a system during a GMD event. The example test system is depicted in Figure 4. CTs and PTs are located at the three-phase buses LEFT, RIGHT and LOAD, measuring the three phase currents and voltages. The parameters of the instrumentation channels are shown in TABLE I. The instrumentation cable is #10 copper cable with the length 100 meters. Burden in CT channels is 0.1Ω and burden in PT channels is 10 kΩ. We focus on two protection zones: (a) the transformer between busses RIGHT and LOAD, and (b) the transmission line between buses LEFT and RIGHT. Several events of geomagnetic disturbance (GMD) and faults are considered. The response of the protection is computed with and without error correction of instrumentation channel errors.

TABLE I. Instrumentation Channels Parameters

Location	CT ratio	PT ratio
Bus LEFT	2000:5	66,400:115
Bus RIGHT	2000:5	66,400:115
Bus LOAD	2000:5	14,400:115

A. Protection Zone 1 – Transformer

Protection zone 1 contains the 115kV/25kV WYE-WYE connected transformer and adjacent breakers. For this protection zone the following events are considered.

Event A-1: At time t=0s, the circuit breaker at bus SRC is closed, and the generator and step up transformer is connected to grid, which energizes the transmission lines and transformers. Before 0s, there is not current flowing in the protection zones. This event focus on the inrush current during transformer energization.

Event A-2: At time t=8s, a GMD events is introduced to the system. The magnitude of the earth electric field is 5V/km and the direction is aligned with the transmission line. The equivalent GMD DC voltage source locates between the groundings of transmission line from bus LEFT to bus RIGHT. The distance between the buses is 20km, so a 100V DC offset is introduced. The GMD event retreats at 18s.

Event A-3: At time t=16s, a Phase A to neutral fault occurs at bus MID. The fault resistance is 0.1Ω and this external fault exists until it is cleared at 16.2s. After 16.2s, the system is recovered, and the phase A of transformer is re-energized. This event focus on this recovery process. During this event, the GMD event is still affecting the system.

In each event, three different EBP relays operate individually to monitor the protection zone. Three phase voltage measurements and three phase current measurements at bus RIGHT and bus LOAD are streamed to the relays. The first EBP works with the direct measurements from primary side, which is the exact value of the voltages and currents at buses. The behavior of this EBP relay is used as a reference. The second EBP works with raw measurements from instrumentation channels, which is the measurements at burden multiplied by the instrumentation transformer ratios. These measurements are vulnerable to error introduced in instrumentational channels. The third EBP works with corrected measurements, which is the result of proposed state estimation based error correction method. Compared with raw measurements, the corrected measurements should be more consistent with the exact value in primary side of the gird. The three EBP use the same tripping decision function in equation (6), in which, $t_{delay} = 10ms$ and $t_{reset} = 300\text{ms}$. In the following results, the performance of three EBP relays are

compared. Figure 5 to Figure 7 provide sample waveforms during these events. The first trace is the voltage of phase A to ground at bus RIGHT. The second trace is the current of phase A at the same bus. Third and fourth traces are the voltage and current of Phase A at bus LOAD.

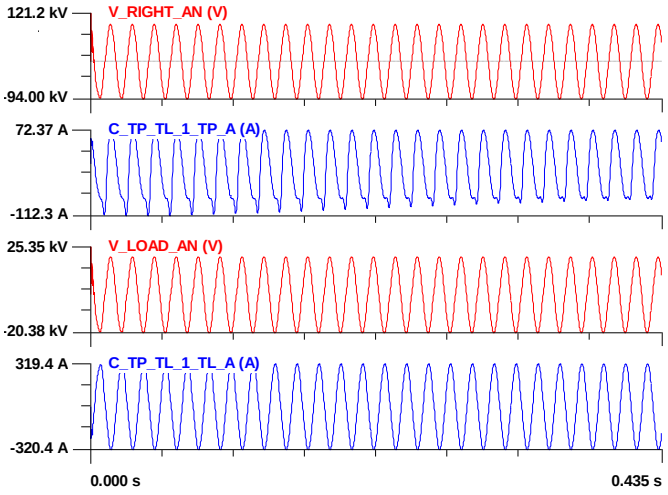

Figure 5. Exact measuremensts in protection zone 1: EVENT A-1

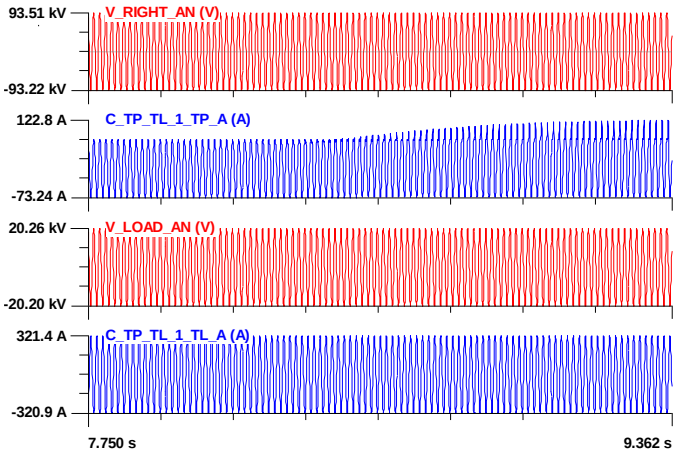

Figure 6. Exact measuremensts in protection zone 1: EVENT A-2

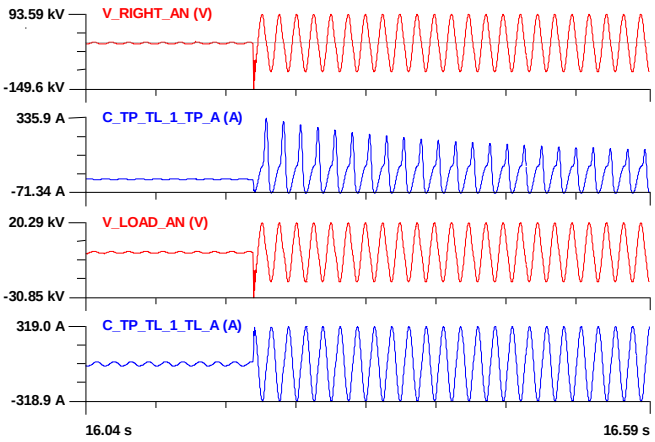

Figure 7. Exact measuremensts in protection zone 1: EVENT A-3

1) Event A-1: Energization of transformer (0~0.4s)

At t=0s, the closer at bus SRC is closed, and the generator and step up transformer are connected the system. Due to the influence of the inrush current of transformer in protection zone, the EBP with simple measurements mis-operates during the beginning of the simulation. The status of EBP from 0 to 0.4s is shown in Figure 8. The increase of chi square value leads to the drop of confidence level. As a result, the EBP mistakenly detects an internal fault. In Figure 9 and Figure 10, the estimated current and voltages at bus RIGHT are compared with the primary value. Also, the measurements without correction are included in the comparison. It is apparent that, the error introduced in voltage channel lead to mis-operation of EBP. Meanwhile, the EBP with corrected measurements does not issue a trip decision as expected.

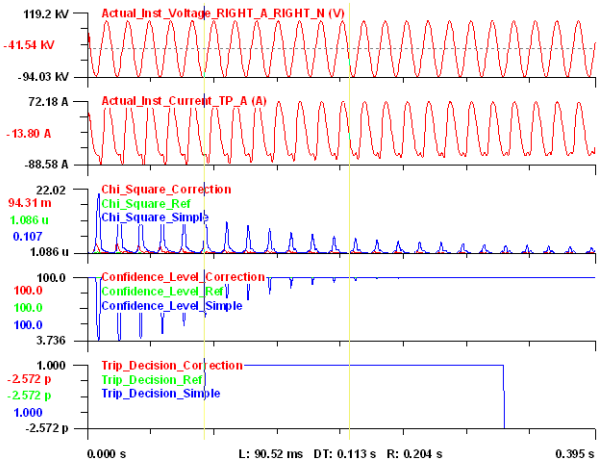

Figure 8. EBP Performance in Protection Zone 1:Event A-1

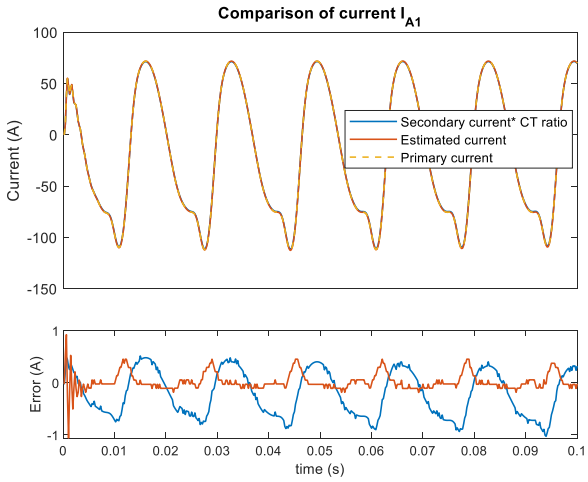

Figure 9. Comparision of currents in event A-1

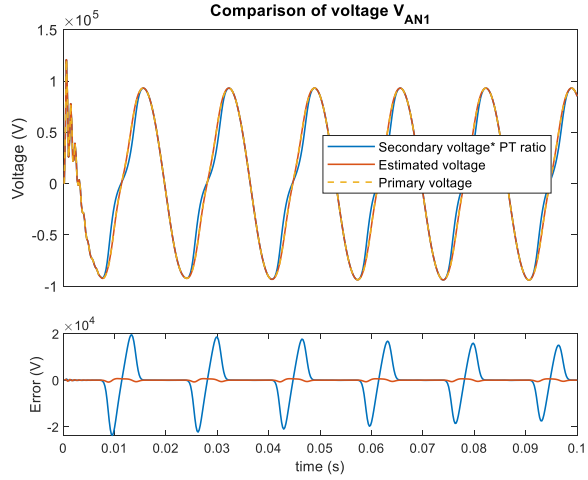

Figure 10. Comparision of voltages in event A-1

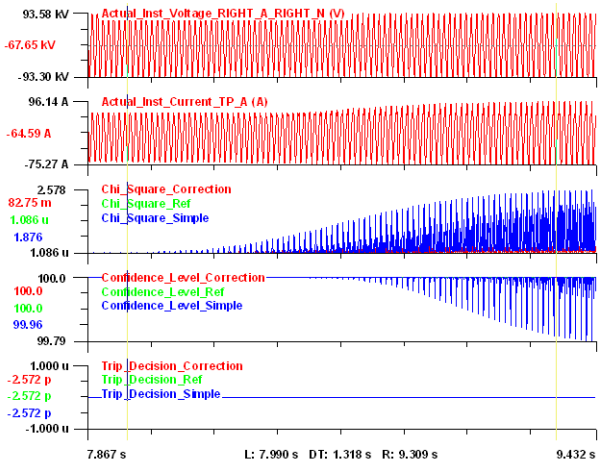

Figure 11. EBP Performance in Protection Zone 1:Event A-2

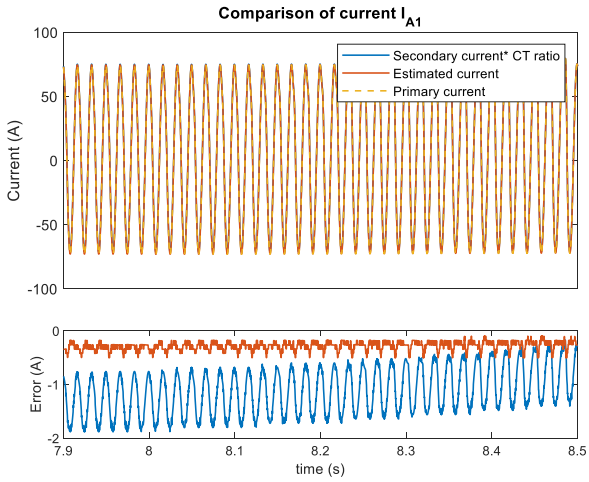

Figure 12. Comparision of currents in event A-2

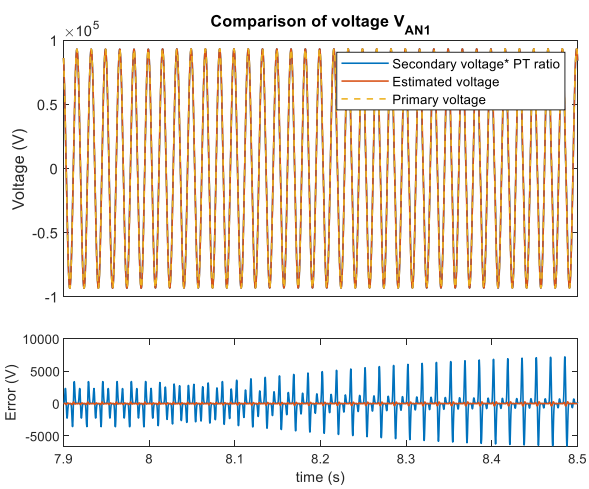

Figure 13. Comparision of voltages in event A-2

2) Event A-2:Onset of GMD events (8s~10s)

To demonstrate the influence of GMD events on the instrumentation channel, a GMD events is introduced during the simulation. The GMD events starts at 8s and ends at 18s. The magnitude of induced electric field is 5V/km, which is modeled as DC voltage source between grounding at bus LEFT and RIGHT. During the beginning of the GMD events, the EBP with simple measurements generates high chi square and low confidence level, which is shown in Figure 11. Though the drop in confidence level does not lead a trip decision, this behavior decreases the reliability of EBP relay. In Figure 12 and Figure 13, the estimated current and voltages at bus RIGHT are compared with the primary value. In this case, the error in voltage channel is the reason of the compromised performance.

3) Event A-3: Re-energization of transformer after fault clearing (16.2s ~16.5s)

At 16s, an external fault at bus MID is introduced, and the fault is cleared at 16.2s. After the external fault was cleared, the EBP with simple measurements mis-operates, which is shown in Figure 14. This mis-operation is similar to the one

occurs at the beginning of the simulation. In both cases, the transformer in protection is energized from offline. In Figure 15 and Figure 16, the estimated current and voltages at bus RIGHT are compared with the primary value. The distorted voltage measurements lead to the mis-operation of EBP.

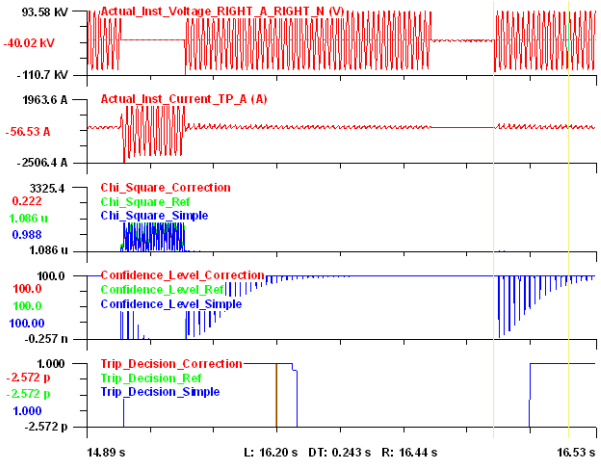

Figure 14. EBP Performance in Protection Zone 1:Event A-3

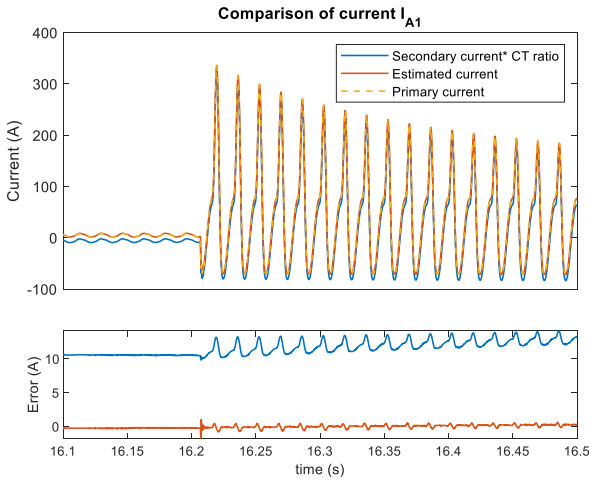

Figure 15. Comparision of currents in event A-3

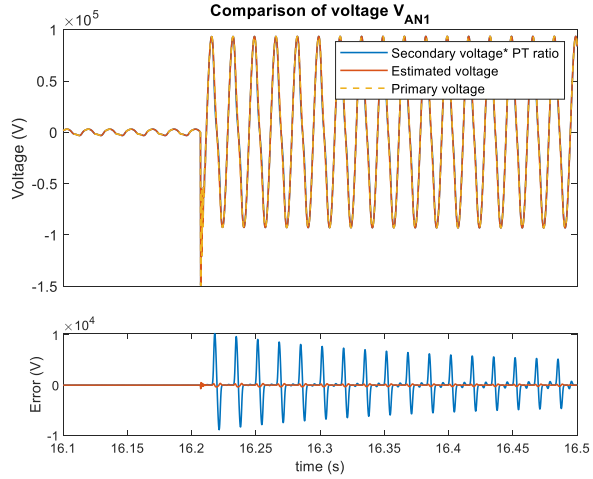

Figure 16. Comparision of voltages in event A-3

B. *Protection Zone 2- Transmission Line*

Protection zone 2 contains the transmission line between buses LEFT and RIGHT, and the line breakers. For this protection zone the following event is considered:

Event B-1: At time t=8s, a GMD events is introduced to the system. The magnitude of the earth electric field is 5V/km. The equivalent GMD DC voltage source locates between the groundings of transmission line from bus LEFT to bus RIGHT. The GMD event retreats at 18s.

In this event, three different EBP relays with different types of measurements operate individually. Three phase voltage measurements and three phase current measurements at bus LEFT and bus RIGHT are streamed to the relays. The configurations of relays are consistent with the relays in protection zone 1. In the following results, the performance of three EBP relays are compared.

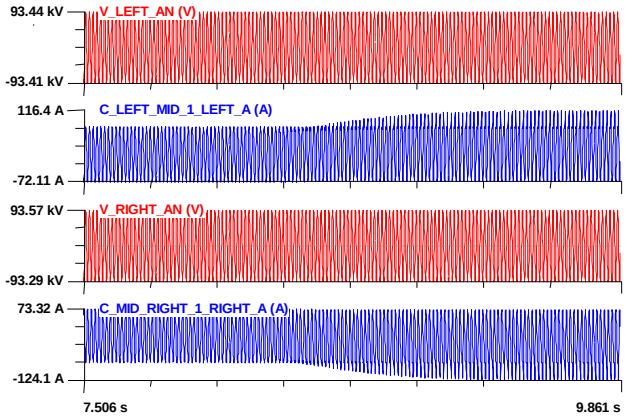

Figure 17. Exact measuremensts in protection zone 2: EVENT B-1

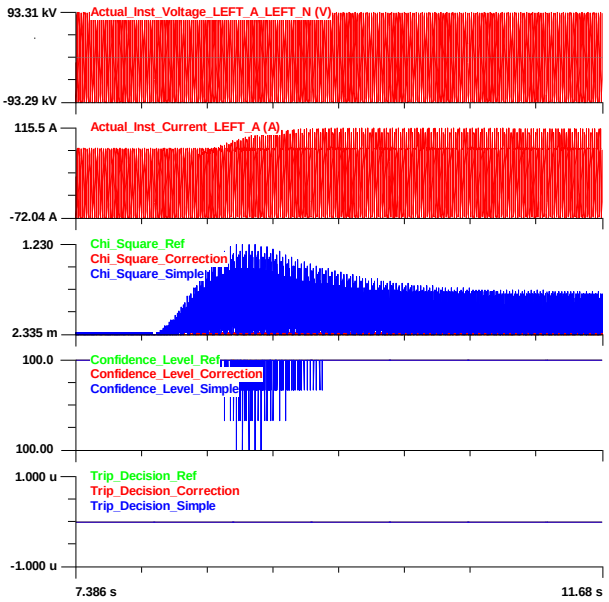

Figure 18. EBP Performance in Protection Zone 2:Event B-1

Figure 17 provides sample waveforms during this event. The first trace is the voltage of phase A to ground at bus LEFT. The second trace is the current of phase A at the same bus. Third and fourth traces are the voltage and current of Phase A at bus RIGHT. Figure 18 shows that due to the increase in chi square, there is a drop in confidence level. Although the magnitude of drop is not large enough for EBP to issue trip decision, this behavior shows the distorted measurements may lead to the mis-operation of EBP.

V. CONCLUSIONS

We presented a high fidelity model for simulating the effects of GIC on power systems. The model is based on detailed representation of power system frequency dependent grounding models, low broadband modeling of transmission lines and transformers models with detailed magnetization characteristics. Using this model we presented examples of effects of Geomagnetic Disturbances on the relaying system for different levels of geomagnetically induced currents into the power system via the grounds of the power systems. The examples show that during these events, DC flow in power transformers generates harmonics and the phase currents are distorted with DC and harmonics. The examples also show that relaying instrumentation channels are affected but these waveforms and can generate substantial errors at the relay input. We presented a method to correct these errors by using a dynamic state estimation. The paper describes the method and presents examples that demonstrate the effectiveness of the method to remove the complex errors introduced by geomagnetically induced currents. Instrumentation channel error correction can substantially improve the reliability of protective relays during a GMD event. The instrumentation channel error correction method works seamlessly with EBP. The simulation tests show that the measurement error introduced in current instrumentation channel and voltage instrumentation channel are eliminated. The corrected measurements facilitate the reliable operation of EBP and avoid the mis-operation of EBP during GMD events.

APPENDIX A: MEASUREMENT MODEL FOR CT CHANNEL

In addition to the magnetizing branch described in Section III-A, the following equations are derived for CT channel measurement model.

KCL at node 0 yields:

$$0 = -g_m e(t) - i_m(t) + \frac{1}{n} i_p(t) + \mathrm{i}_{L_1}(t) + g_{s1} L_1 \frac{di_{L_1}(t)}{dt}$$

KCL at node 1 yields:

$$0 = g_m e(t) + i_m(t) - \frac{1}{n} i_p(t) - \mathrm{i}_{L_2}(t) - g_{s2}\left(L_2 \frac{di_{L_2}(t)}{dt} - M_{23} \frac{di_{L_3}(t)}{dt} \right)$$

KCL at node 2 yields:

$$0 = -g_m e(t) - i_m(t) + \frac{1}{n} i_p(t) + \mathrm{i}_{L_3}(t) + g_{s3}\left(L_3 \frac{di_{L_3}(t)}{dt} - M_{23} \frac{di_{L_2}(t)}{dt} \right)$$

KVL loop: node 1 to transformer to node 2, yields:

$$0 = -v_1(t) + v_2(t) + e(t) + L_1 \frac{di_{L_1}(t)}{dt} + r_1\left(g_m e(t) + i_m(t) - \frac{1}{n} i_p(t) \right)$$

KVL loop: node 3 to node 1, yields:

$$0 = -v_3(t) + v_1(t) + r_2\left(\mathrm{i}_{L_2}(t) + g_{s2}\left(L_2 \frac{di_{L_2}(t)}{dt} - M_{23} \frac{di_{L_3}(t)}{dt} \right) \right) + L_2 \frac{di_{L_2}(t)}{dt} - M_{23} \frac{di_{L_3}(t)}{dt}$$

KVL loop: node 2 to node 4, yields:

$$0 = -v_2(t) + v_4(t) + r_3\left(\mathrm{i}_{L_3}(t) + g_{s3}\left(L_3 \frac{di_{L_3}(t)}{dt} - M_{23} \frac{di_{L_2}(t)}{dt} \right) \right) + L_3 \frac{di_{L_3}(t)}{dt} - M_{23} \frac{di_{L_2}(t)}{dt}$$

KCL at node 3 yields:

$$0 = \mathrm{i}_{L_2}(t) + g_{s2}\left(L_2 \frac{di_{L_2}(t)}{dt} - M_{23} \frac{di_{L_3}(t)}{dt} \right) + g_b\left(v_3(t) - v_4(t) \right)$$

KCL at node 4 yields:

$$0 = -\mathrm{i}_{L_3}(t) - g_{s3}\left(L_3 \frac{di_{L_3}(t)}{dt} - M_{23} \frac{di_{L_2}(t)}{dt} \right) + g_b\left(v_4(t) - v_3(t) \right)$$

Transformer magnetizing leg yields:

$$0 = e(t) - \frac{d\lambda(t)}{dt}$$

Aforementioned 14 measurements derived from physical laws are referred as virtual measurements. Apart from virtual measurements, we have the following measurements to improve the redundancy of the scheme.

Actual Measurements (1):

$$v_{out}(t) = v_3(t) - v_4(t)$$

Pseudo Measurements (1):

node 4 is grounded:

$$0^m = v_4(t)$$

Derived Measurements (4):

$$i_b^m(t) = g_m e(t) + \mathrm{i}_m(t) - \frac{1}{n} i_p(t)$$

$$i_b^m(t) = \mathrm{i}_{L_1}(t) + g_{s1} L_1 \frac{di_{L_1}(t)}{dt}$$

$$i_b^m(t) = \mathrm{i}_{L_2}(t) + g_{s2}\left(L_2 \frac{di_{L_2}(t)}{dt} - M_{23} \frac{di_{L_3}(t)}{dt} \right)$$

$$i_b^m(t) = -\mathrm{i}_{L_3}(t) - g_{s3}\left(L_3 \frac{di_{L_3}(t)}{dt} - M_{23} \frac{di_{L_2}(t)}{dt} \right)$$

In which, $i_b^m(t) = -g_b\left(v_3(t) - v_4(t) \right)$

APPENDIX B: MEASUREMENT MODEL FOR PT CHANNEL

Actual Measurements (1):

$$V_{out}(t) = v_5(t) - v_6(t)$$

Pseudo Measurements (2):

node 2 and node 4 are grounded:

$0 = v_2(t)$, $0 = v_4(t)$

Virtual Measurements (18):

KCL at node 1, node 2 and node 4 yields:

$0 = i_1(t) + i_2(t) + i_4(t) + i_6(t)$, in which:

$$i_1(t) = i_{L1}(t) + g_s L_1 \frac{di_{L1}(t)}{dt} + C_1 \frac{dv_{c1}(t)}{dt} + C_3 \frac{dv_{c3}(t)}{dt}$$

$$i_2(t) = -i_{L1}(t) - g_s L_1 \frac{di_{L1}(t)}{dt} - C_1 \frac{dv_{c1}(t)}{dt}$$

$$i_4(t) = -i_{L2}(t) - g_s L_2 \frac{di_{L2}(t)}{dt} - C_2 \frac{dv_{c2}(t)}{dt}$$

$$i_6(t) = (G_{21} + G_{s21}) v_3(t) + (G_{22} + G_{s22}) v_4(t) - G_{s21} v_5(t) - G_{s22} v_6(t) + C_{21} \frac{dv_3(t)}{dt} + C_{22} \frac{dv_4(t)}{dt} + i_{L4}(t)$$

KCL at node 3 yields:

$0 = i_3(t) + i_5(t)$, in which:

$$i_3(t) = i_{L2}(t) + g_s L_2 \frac{di_{L2}(t)}{dt} + C_2 \frac{dv_{c2}(t)}{dt} - C_3 \frac{dv_{c3}(t)}{dt}$$

$$i_5(t) = (G_{11} + G_{s11}) v_3(t) + (G_{12} + G_{s12}) v_4(t) - G_{s11} v_5(t) - G_{s12} v_6(t) + C_{11} \frac{dv_3(t)}{dt} + C_{12} \frac{dv_4(t)}{dt} + i_{L3}(t)$$

KCL at node 5 yields:

$0 = i_7(t) + i_9(t)$, in which:

$$i_7(t) = (G_{11} + G_{s11}) v_5(t) + (G_{12} + G_{s12}) v_6(t) - G_{s11} v_3(t) - G_{s12} v_4(t) + C_{11} \frac{dv_5(t)}{dt} + C_{12} \frac{dv_6(t)}{dt} - i_{L3}(t)$$

$$i_9(t) = v_5(t) / R_b - v_6(t) / R_b$$

KCL at node 6 yields:

$0 = i_8(t) + i_{10}(t)$, in which:

$$i_8(t) = (G_{21} + G_{s21}) v_5(t) + (G_{22} + G_{s22}) v_6(t) - G_{s21} v_3(t) - G_{s22} v_4(t) + C_{21} \frac{dv_5(t)}{dt} + C_{22} \frac{dv_6(t)}{dt} - i_{L4}(t)$$

$$i_{10}(t) = -v_5(t) / R_b + v_6(t) / R_b$$

KVL loops yield:

$$0 = v_1(t) - v_2(t) - e(t) - L_1 \frac{di_{L1}(t)}{dt} - r_1 \left(i_{L1}(t) + g_s L_1 \frac{di_{L1}(t)}{dt} \right)$$

$$0 = v_3(t) - v_4(t) - \frac{1}{N} e(t) - L_2 \frac{di_{L2}(t)}{dt} - r_2 \left(i_{L2}(t) + g_s L_2 \frac{di_{L2}(t)}{dt} \right)$$

$$0 = v_1(t) - v_2(t) - v_{c1}(t) - r_{s1} C_1 \frac{dv_{c1}(t)}{dt}$$

$$0 = v_1(t) - v_3(t) - v_{c3}(t) - r_{s3} C_3 \frac{dv_{c3}(t)}{dt}$$

$$0 = v_2(t) - v_4(t) - v_{c2}(t) - r_{s2} C_2 \frac{dv_{c2}(t)}{dt}$$

$$0 = i_{L1}(t) + g_s L_1 \frac{di_{L1}(t)}{dt} - i_c(t) - i_m(t) - g_c e(t)$$

$$0 = N i_c(t) + i_{L2}(t) + g_s L_2 \frac{di_{L2}(t)}{dt}$$

$$0 = -v_3(t) + v_5(t) + R_{11} i_{L3}(t) + R_{12} i_{L4}(t) + L_{11} \frac{di_{L3}(t)}{dt} + L_{12} \frac{di_{L4}(t)}{dt}$$

$$0 = -v_4(t) + v_6(t) + R_{21} i_{L3}(t) + R_{22} i_{L4}(t) + L_{21} \frac{di_{L3}(t)}{dt} + L_{22} \frac{di_{L4}(t)}{dt}$$

Transformer magnetizing leg yields:

$$0 = e(t) - \frac{d\lambda(t)}{dt}$$

$$0 = i_m(t) - i_0 \frac{\lambda(t)}{\lambda_0} y_3(t) - \frac{1}{L_0} \lambda(t)$$

$$0 = y_1(t) - \frac{\lambda(t)^2}{\lambda_0^2}$$

$$0 = y_2(t) - y_1(t)^2$$

$$0 = y_3(t) - y_2(t)^2$$

REFERENCES

[1] J. Pan, K. Vu, and Y. Hu, "An Efficient Compensation Algorithm for Current Transformer Saturation Effects," *IEEE Trans. Power Deliv.*, vol. 19, no. 4, pp. 1623–1628, Oct. 2004.

[2] A. P. S. Meliopoulos *et al.*, "Dynamic State Estimation-Based Protection: Status and Promise," *IEEE Trans. Power Deliv.*, vol. 32, no. 1, pp. 320–330, Feb. 2017.

[3] J. Xie, A.P. Meliopoulos, and Y. Liu, "Low Broadband Transmission Line Model for Geomagnetically Induced Current Analysis," in *2018 IEEE Power & Energy Society General Meeting*, 2018.

[4] A. P. S. Meliopoulos, J. Xie, and G. Cokkinides, "Power system harmonic analysis under geomagnetic disturbances," presented at the 2018 18th International Conference on Harmonics and Quality of Power (ICHQP), 2018, pp. 1–6.

[5] A. P. S. Meliopoulos, G. Cokkinides, J. Xie, and Y. Kong, "Instrumentation Error Correction within Merging Units," in *Proceedings of the 2018 Georgia Tech Fault and Disturbance Analysis Conference*, 2018.

[6] C.-S. Yu, "Detection and Correction of Saturated Current Transformer Measurements Using Decaying DC Components," *IEEE Trans. Power Deliv.*, vol. 25, no. 3, pp. 1340–1347, Jul. 2010.

[7] T. K. Hamrita, B. S. Heck, and A. P. S. Meliopoulos, "On-line correction of errors introduced by instrument transformers in transmission-level steady-state waveform measurements," *IEEE Trans. Power Deliv.*, vol. 15, no. 4, pp. 1116–1120, Oct. 2000.

[8] G. K. Stefopoulos, G. J. Cokkinides, and A. P. Meliopoulos, "Quadratic integration method for transient simulation and harmonic analysis," in *Harmonics and Quality of Power, 2008. ICHQP 2008. 13th International Conference on*, 2008, pp. 1–6.